The Meteoritical Society

Meteoritics & Planetary Science 1–17 (2015)
doi: 10.1111/maps.12449

Sulfur in presolar silicon carbide grains from asymptotic giant branch stars

Peter HOPPE[1*], Katharina LODDERS[2], and Wataru FUJIYA[1]

[1]Max Planck Institute for Chemistry, Hahn-Meitner-Weg 1, 55128 Mainz, Germany
[2]Department of Earth & Planetary Sciences and McDonnell Center for the Space Sciences, Washington University, Campus Box 1169, St. Louis, Missouri 63130, USA
[*]Corresponding author. E-mail: peter.hoppe@mpic.de

(Received 28 July 2014; revision accepted 25 February 2015)

Abstract–We studied 14 presolar SiC mainstream grains for C-, Si-, and S-isotopic compositions and S elemental abundances. Ten grains have low levels of S contamination and CI chondrite-normalized S/Si ratios between 2×10^{-5} and 2×10^{-4}. All grains have S-isotopic compositions compatible within 2σ of solar values. Their mean S isotope composition deviates from solar by at most a few percent, and is consistent with values observed for the carbon star IRC+10216, believed to be a representative source star of the grains, and the interstellar medium. The isotopic data are also consistent with stellar model predictions of low-mass asymptotic giant branch (AGB) stars. In a $\delta^{33}S$ versus $\delta^{34}S$ plot the data fit along a line with a slope of 1.8 ± 0.7, suggesting imprints from galactic chemical evolution. The observed S abundances are lower than expected from equilibrium condensation of CaS in solid solution with SiC under pressure and temperature conditions inferred from the abundances of more refractory elements in SiC. Calcium to S abundance ratios are generally above unity, contrary to expectations for stoichiometric CaS solution in the grains, possibly due to condensation of CaC_2 into SiC. We observed a correlation between Mg and S abundances suggesting solid solution of MgS in SiC. The low abundances of S in mainstream grains support the view that the significantly higher abundances of excess ^{32}S found in some Type AB SiC grains are the result of in situ decay of radioactive ^{32}Si from born-again AGB stars that condensed into AB grains.

INTRODUCTION

Primitive meteorites and interplanetary dust particles contain small quantities (up to several 100 ppm) of refractory dust grains that formed in the winds of evolved stars and in the ejecta of stellar explosions (Zinner 2014). These grains are older than our solar system and therefore they have been named presolar grains. Presolar grains can be distinguished from matter that was processed in the early solar system by their large isotopic anomalies in major and minor elements. Among the presolar minerals identified to date are silicon carbide (SiC) (Bernatowicz et al. 1987; Tang and Anders 1988); graphite (Amari et al. 1990); silicon nitride (Si_3N_4) (Nittler et al. 1995); oxides, e.g., corundum and other forms of Al_2O_3 and spinel (Hutcheon et al. 1994; Nittler et al. 1994); and silicates (Messenger et al. 2003). These grains have typical sizes of several 100 nm, and a small fraction of them has sizes in the micrometer-range. Other presolar minerals, e.g., TiC, have been identified as subgrains enclosed in larger SiC and graphite grains (Bernatowicz et al. 1991; Croat et al. 2003).

Laboratory studies of individual presolar grains can provide information on stellar nucleosynthesis and evolution, mixing in supernova ejecta, galactic chemical evolution (GCE), grain formation in stellar environments, processing of dust in the interstellar medium (ISM), the types of stars that contributed dust to our solar system, and materials processing in early solar system history. A key instrument for isotope studies of the light and intermediate-mass elements in presolar grains is the NanoSIMS ion probe (Hoppe et al. 2013). This new generation secondary ion mass spectrometer has multi-collection capability, high sensitivity at high mass resolution, and permits isotope

and elemental abundance measurements with spatial resolution down to 50 nm for Cs^+ primary ions and down to 200 nm for O^- primary ions. Important complementary analysis techniques are resonance ionization mass spectrometry (RIMS) for isotope analyses of intermediate-mass and heavy elements (e.g., Nicolussi et al. 1997) and transmission electron microscopy (TEM) for mineralogical studies of electron-transparent sections prepared by microtomy or focused ion beam (FIB) technique (Croat et al. 2003; Zega et al. 2007; Holzapfel et al. 2008).

Silicon carbide is the best characterized presolar mineral because (1) it can be separated from meteorites by physical and chemical treatments in almost pure form, (2) it is relatively abundant (typically 10s of ppm), and (3) it has relatively high concentrations of elements other than C and Si (e.g., up to several wt% N, 500–1000 ppm Zr [20–40× CI], and 15–40 ppm Ba [10–30× CI] in submicrometer-sized grains; Amari et al. 1995). Based on the isotopic compositions of C, N, and Si presolar SiC is divided into eight distinct populations (Zinner 2014). Most abundant are the mainstream (MS) grains which make up about 90% of all grains. These grains have $^{12}C/^{13}C$ ratios between 10 and 100 and only moderate Si isotope anomalies of several percent. In a $\delta^{29}Si$ versus $\delta^{30}Si$ plot[1] the MS grains plot along a characteristic line with slope 1.37 (MS line; Zinner et al. 2007). Mainstream grains are believed to come from 1.5–3 $M_\odot$ asymptotic giant branch (AGB) stars of about solar metallicity[2] (Lugaro et al. 2003). The Type Y and Z grains (a few percent of all known SiC grains) are thought to come from intermediate-mass AGB stars of subsolar metallicities as concluded from their C and Si isotope ratios (Hoppe et al. 1997; Amari et al. 2001b). SiC grains with $^{12}C/^{13}C$ ratios <10 are very rare nova grains or the Type AB grains that constitute a few percent of SiC (Amari et al. 2001a, 2001c). The origin of the AB grains is still a matter of debate and among the proposed stellar sources are J-type carbon stars (Lambert et al. 1986) and born-again AGB stars, such as Sakurai's object (Asplund et al. 1999). The rare (1–2% of all SiC) Type X and C grains formed in the ejecta of Type II supernova (SN) explosions. The SN X grains exhibit strong enrichments in ^{28}Si, whereas the C grains show large enrichments in the heavy Si isotopes. Although there are always exceptions to the rule, other common characteristics of SiC from SN ejecta are supersolar $^{12}C/^{13}C$ ratios, subsolar $^{14}N/^{15}N$ ratios, and large ^{32}S enrichments (especially in the C grains), and, inferred from large isotopic overabundances of ^{26}Mg and ^{44}Ca, incorporation of high abundances of radioactive ^{26}Al (half-life 716,000 yr) and ^{44}Ti (half-life 60 yr) (Nittler et al. 1996; Hoppe et al. 2000, 2012; Lin et al. 2010).

Other elements in the SiC grains can be depleted relative to solar (e.g., Mg, Ca, and Fe), solar-like (e.g., Ti), or enriched (e.g., Zr, Ba) in MS grains (Amari et al. 1995). Their isotopic compositions, especially those of the heavy s-process elements (e.g., Nicolussi et al. 1997), have played a key role for identifying the stellar sources of MS grains. The elemental abundance patterns can be used to constrain the conditions under which the SiC grains condensed, e.g., C/O ratio, pressure, and temperature. Element abundances in SiC are determined by two factors, their abundances in the atmosphere of the parent star and their condensation behavior into SiC. Many of the elemental abundance patterns of MS grains are well matched by condensation calculations for C-rich stellar atmospheres (Lodders and Fegley 1995), in agreement with the proposed origin from low-mass C-rich AGB stars of about solar metallicity.

The recent discovery of S isotope anomalies in presolar SiC grains is particularly interesting for further studies. Large enrichments in ^{32}S have not only been found in SN grains (Gyngard et al. 2010; Hoppe et al. 2012; Xu et al. 2012) but recently also in three AB grains (Fujiya et al. 2013). Born-again AGB stars, which are among the proposed stellar sources of AB grains, are predicted to produce significant amounts of radioactive ^{32}Si (half-life 153 yr) and the ^{32}S excesses may be the result of in situ ^{32}Si decay (Fujiya et al. 2013). This was proposed also for the SN C grains (Pignatari et al. 2013) but a SN origin of AB grains with ^{32}S excesses is considered unlikely because of missing evidence for ^{44}Ti, relatively low $^{26}Al/^{27}Al$ ratios (a few times 10^{-3}), and radiogenic ^{32}S along with low $^{12}C/^{13}C$ ratios (Fujiya et al. 2013). The ^{32}S enrichments observed in AB grains (~250 ‰) are lower than those in C grains and an origin through ^{32}Si decay that had condensed into SiC is less secured. There is the alternative possibility that the ^{32}S enrichments in AB grains are the signature of the initial S-isotopic composition in their parent stars. The parent stars do not have to be solar in S-isotopic compositions and could show trends as observed for the Si-isotopic compositions of AB and MS grains. The observed range of Si-isotopic compositions in AB and MS grains ($\delta^{29}Si = -50 \ldots +200‰$, $\delta^{30}Si = -50 \ldots +150‰$) is interpreted to be the fingerprint of GCE, but the exact processes have not been unambiguously identified yet (see the Discussion section in Nittler and Dauphas 2006). It is conceivable that GCE has left a similar fingerprint on S-isotopic compositions, which is expected from models of GCE. These predict variations of $^{33,34}S/^{32}S$ ratios of ~100‰ for $-0.15 < [Fe/H] \leq 0$,

[1] $\delta^i Si = ([^iSi/^{28}Si]_{sample}/[^iSi/^{28}Si]_\odot - 1) \times 1000$.
[2] Metallicity is the mass fraction of elements heavier than He.

(where [Fe/H] = log[Fe/H] − log[Fe/H]$_\odot$) which corresponds to metallicities between 0.7× and 1× solar (Kobayashi et al. 2011). Sulfur-isotopic measurements on nine very large (>7 μm) SiC grains from the Murchison LS + LU series with moderate variations in Si-isotopic ratios of about 50‰ yielded $\delta^{33}S^3$ values from −45‰ to +1‰ and $\delta^{34}S$ values between −44‰ and −2‰ (Gyngard et al. 2007; Hynes and Gyngard 2009) suggesting initial S-isotopic compositions are relatively close to solar in the parent stars. Gyngard et al. (2007) speculated that the true S isotope anomalies might be even smaller. This is because the measurements on their S isotope standard were not corrected for the quasi-simultaneous arrivals (QSA) effect (Slodzian et al. 2001), which could have resulted in an improper correction of instrumental mass fractionation in the NanoSIMS.

Here, we report on S isotope and abundance measurements on 14 SiC MS grains with sizes between 1 and 6 μm from a newly prepared Murchison SiC residue. These analyses (1) increase the yet small data base on S-isotopic compositions of SiC MS grains, (2) expand S isotope measurements to smaller MS grains, (3) measure MS grains with a larger range of Si-isotopic ratios to check for potential GCE effects, and (4) determine elemental S abundances. Sulfur abundances will be compared with predictions from equilibrium condensation calculations and these data will be used to put further constraints on the origin of ^{32}S enrichments in AB grains (radiogenic versus GCE). As MgS and CaS may play important roles for S condensation into SiC, abundances of Ca and Mg were measured as well. Preliminary results of this work were reported in a conference abstract by Hoppe et al. (2014).

EXPERIMENTAL

Sample Preparation

We separated presolar SiC grains from the Murchison CM2 meteorite following the procedure of Besmehn and Hoppe (2003), which is a variant form of the procedure developed by Amari et al. (1994). A ~48 g sample of Murchison (ME 2644 spp. #28.21, Field Museum Chicago) was crushed and split into two parts (A, B) of approximately equal size. Both samples were treated with HCl, HF, CS_2, $Na_2Cr_2O_7$, H_2SO_4 to produce a diamond/SiC/graphite/oxide residue. The diamonds were separated as a colloid in NH_4OH. The remaining SiC/graphite/oxide residue of sample B was further treated with $HClO_4$, H_2SO_4, and HF/HCl to produce the SiC sample (Mur2012B). Several thousand grains from this residue were transferred to ultra-clean Au foils (99,999% Au, cleaned with ethanol and HCl) in a 4:1 isopropanol-water suspension (adjusted with HCl for pH = 4), followed by Argon plasma cleaning (Diener Electronic Pico, 0.3 mbar, 53% power, 1 min) to remove surface contamination delivered with the suspension. Two Au mounts (Mur2012B-3/4) were scanned in a Leo 1530 FE-SEM at Max Planck Institute for Chemistry for SiC grains. Most SiC grains are submicrometer in size but we identified six micrometer-sized SiC grains (3–7 μm) on mount Mur2012B-3 and 46 micrometer-sized (1–6 μm) SiC grains on mount Mur2012B-4 which are potential targets for C, Si, and S isotope measurements.

Isotope Measurements

We measured 23 micrometer-sized SiC grains from mount Mur2012B-4 for their C- and Si-isotopic composition with the Cameca NanoSIMS 50 ion probe at the MPI for Chemistry (Hoppe et al. 2013). Preference was given to grains with relatively compact appearance and smooth surface textures to minimize contributions of S contamination to the S-isotopic measurements. High-resolution ion images of $^{12}C^-$, $^{13}C^-$, $^{28}Si^-$, $^{29}Si^-$, and $^{30}Si^-$, produced by rastering a ~1 pA primary Cs^+ beam (<100 nm size, 16 keV energy) over 2–9 × 2–9 μm^2 sized areas, were recorded in multi-collection mode (256 × 256 pixels, total integration time ~5.5 min, 1 image plane). The measurements were done with an entrance slit width of 30 μm and exit slits widths of 50 μm (^{13}C) and 80 μm (all other species), respectively. This guarantees that all relevant isobaric interferences, especially ^{12}CH and ^{28}SiH, are sufficiently separated. Carbon- and Si-isotopic compositions were normalized to our in-house SiC standard ($\delta^{13}C_{PDB} = -29.1 \pm 1.2$‰, $\delta^{29,30}Si = 0$). The C- and Si-isotopic ratios were corrected for QSA (Slodzian et al. 2001), using QSA constants of 1 for C, and 0.6 for Si (Hoppe et al. 2013). This resulted in corrections of typically a few permil.

We selected 14 MS grains from the set above for S isotope measurements, based on their C- and Si-isotopic signatures. Prior to S isotope measurements, the SiC grains and their surroundings were cleaned with an intense primary Cs^+ ion beam (~25 pA for 5–20 min and raster size somewhat larger than the grain size). This intense presputtering was not able to completely remove surface contamination due to topographic effects of the grains. This is shown in Figs. 1 and 2 by the presence of local S hotspots on grain surfaces or increased S abundances correlating with grain surface textures. Sulfur isotope measurements were done by recording high-resolution ion images of $^{28}Si^-$, $^{32}S^-$,

[3] $\delta^iS = ([^iS/^{32}Si]_{sample}/[^iS/^{32}S]_\odot - 1) \times 1000$.

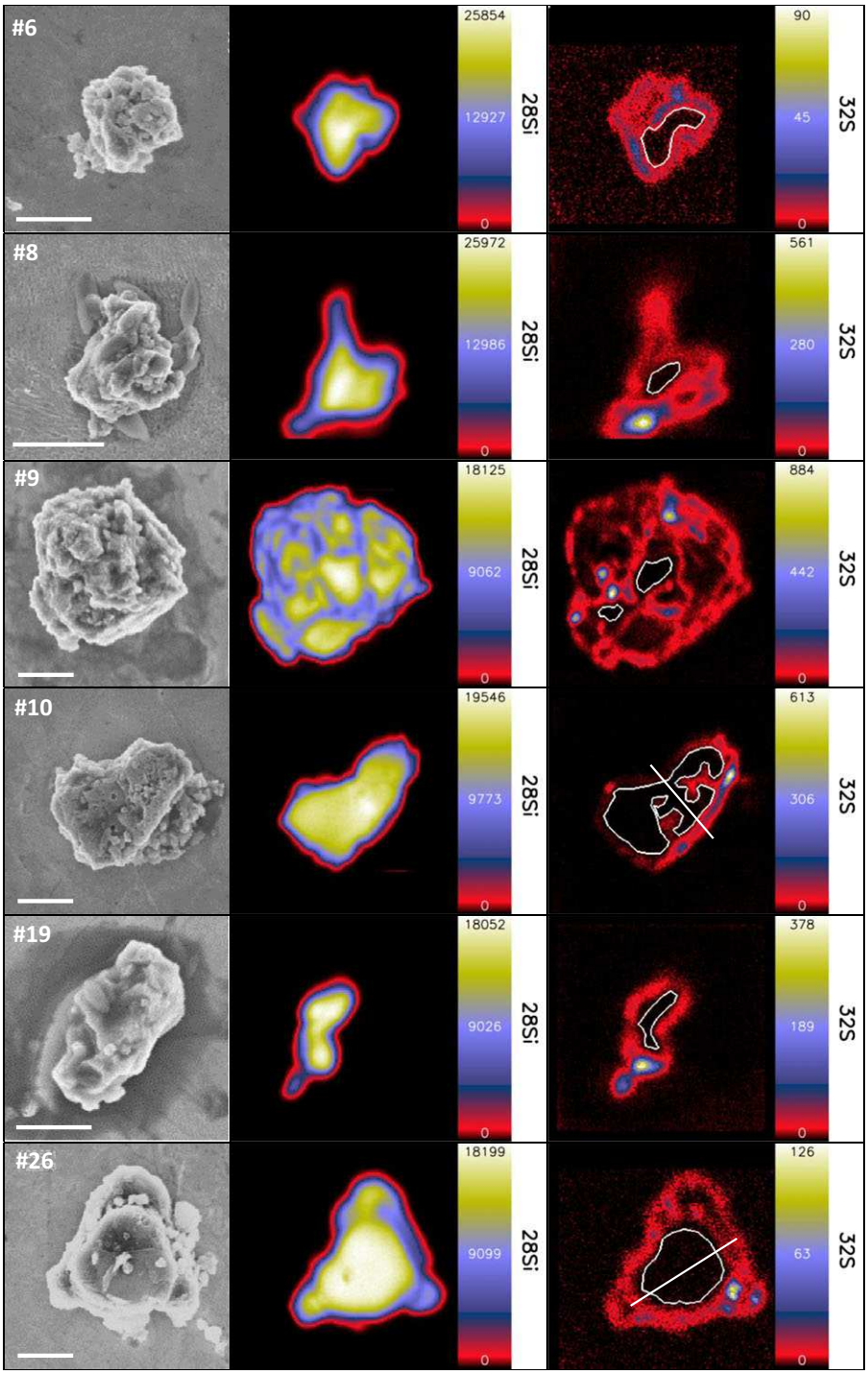

Fig. 1. SEM photographs and NanoSIMS ion images (integrated over 19–30 planes) of $^{28}Si^-$ and $^{32}S^-$ of 14 presolar SiC MS grains (1–6 μm) from the Murchison meteorite. Note that the colors in the ion images (white-yellow-blue-red-black; see web version of this article) are selected for each image individually such that the maximum value (or up to 2 times the maximum value in some $^{32}S^-$ images) is shown in white and the minimum value in black. The scale bars in the SEM images represent 1 μm and also apply to the corresponding ion images. The white outlines in the ^{32}S ion images show areas from which S isotope and abundance data were inferred, assumed to be largely free of S contamination. The two lowest panels show profiles of ^{32}S for grains #10 and #26 along the lines drawn in the respective ion images. Each point in the line profiles represent a superposition of 4 × 4 (#26) and, respectively, 2 × 2 (#10) pixels. The two vertical lines show the intersection with the outline of the low S area.

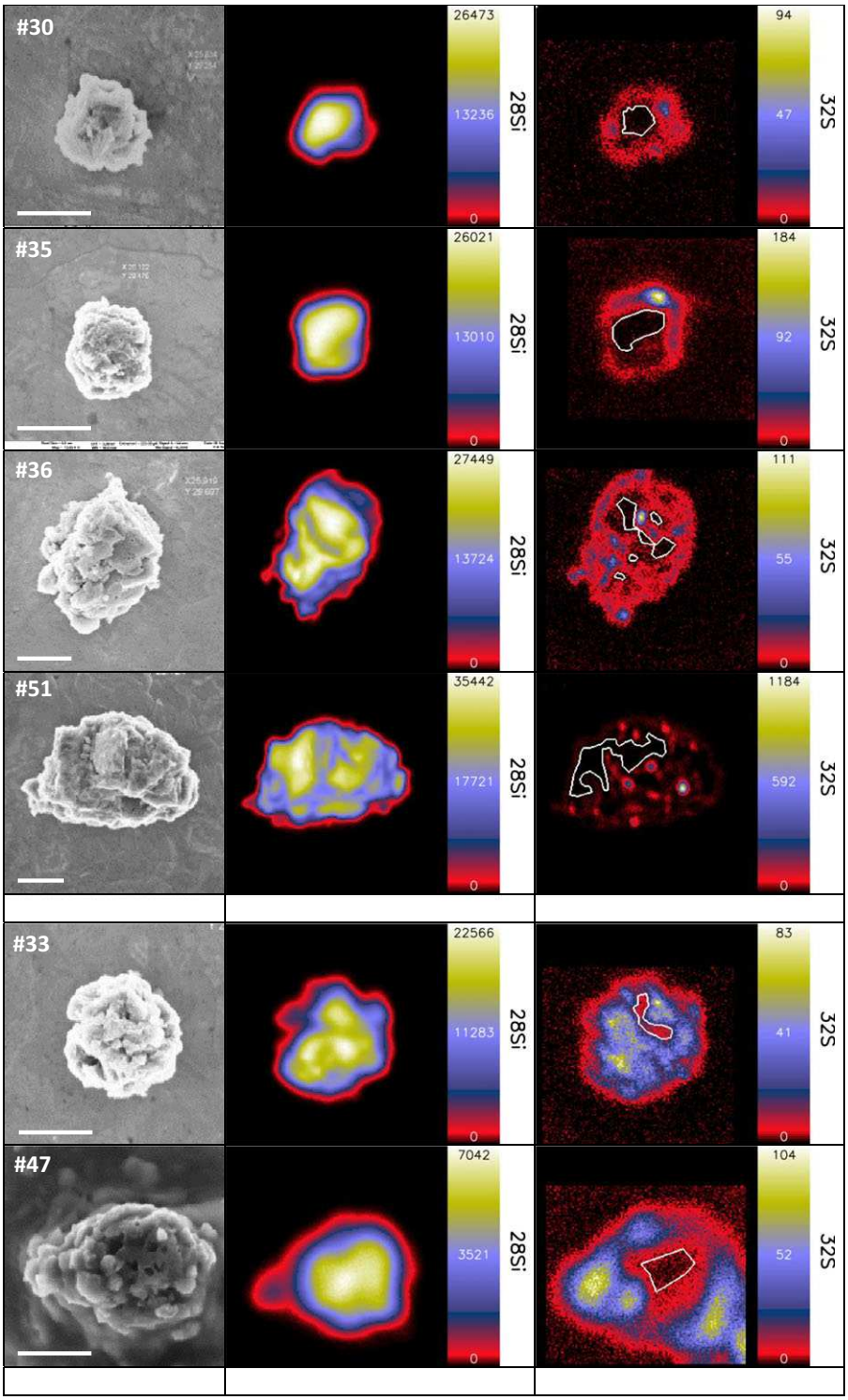

Fig. 1. (Continued).

$^{33}S^{-}$, and $^{34}S^{-}$ in a setup similar to that of the C and Si isotope measurements, but with longer integration times to compensate for the lower S concentrations in the grains (256 × 256 pixels, total integration time ~100–160 min grain^{-1}, divided into 19–30 image planes). Sulfur-36 was not included in our measurements because of its extremely low abundance, which makes it impossible to obtain useful results. Despite long integration times and intense cleaning sufficient material was left to measure Mg and Ca abundances. The

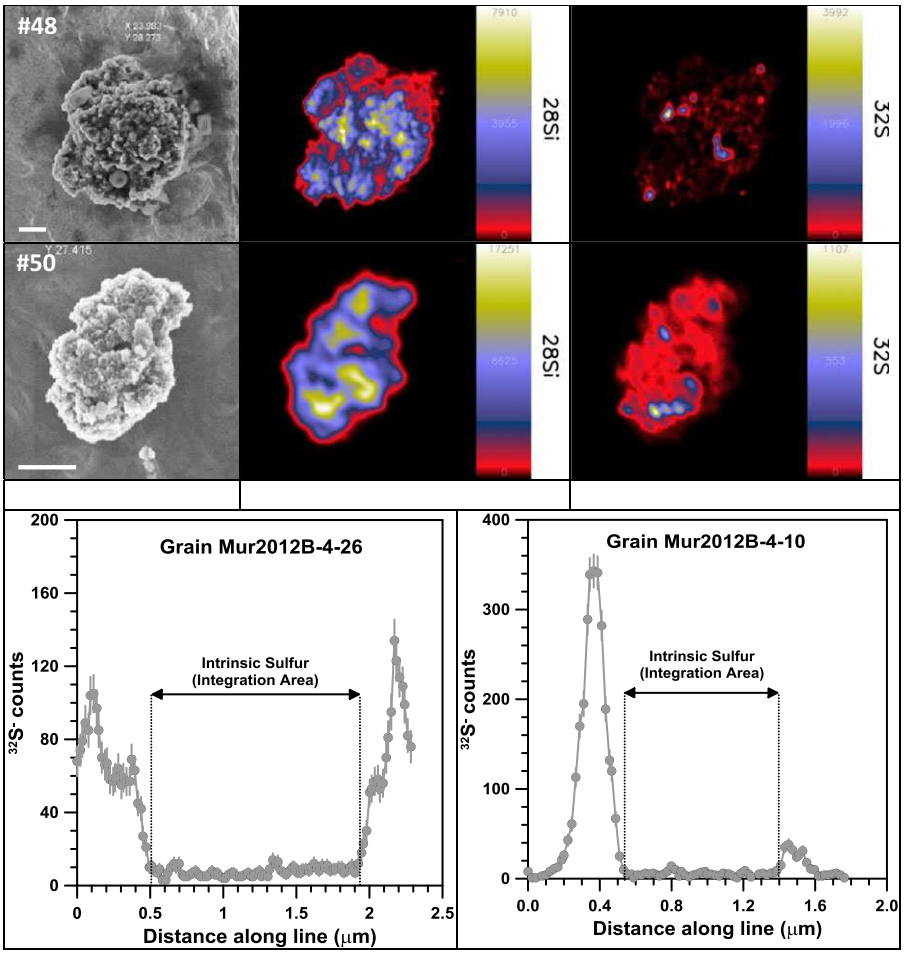

Fig. 1. (Continued).

estimated material consumption (sputter depth) was <400 nm after completion of the C, Si, and S measurements. This depth was inferred from measurements of depth profiles for implanted B in a synthetic SiC standard which gave a sputter rate of 0.094 nm*μm^2 s^{-1} pA^{-1} Cs$^+$ (^{11}B peak at 365 nm, reached after 877 s with 15 × 15 μm^2 raster and 1 nA Cs$^+$ current). This corresponds to a sputter yield of 1.4 atoms/primary ion which is a factor of ~1.5 lower than what was inferred by Wilson et al. (1989) for a Si target and normal incidence of 10 keV Cs$^+$ primary ions. The S isotope measurements were done with an entrance slit width of 20 or 30 μm and exit slits widths of 50 μm (^{33}S) and 80 μm (all other species), respectively. This guarantees that all relevant isobaric interferences, especially ^{32}SH, are sufficiently separated. Sulfur-isotopic compositions were normalized to S contained in our in-house SiC standard which was assumed to have normal, i.e., VCDT S-isotopic composition (^{33}S/^{32}S = 0.0078773, ^{34}S/^{32}S = 0.0441626; Ding et al. 2001). A QSA correction (inferred to be <1‰) was not applied to our data because of low S concentrations, not only in the presolar SiC grains but also in our SiC standard. In contrast, a correction for detector background is more critical, especially for ^{33}S. Detector background was found to be between 0.001 and 0.01 cps, which compares with a typical ^{33}S$^-$ ion signal intensity of 0.15 cps in low S areas of the SiC grains.

Elemental Abundance Measurements

Sulfur abundances were derived from the ^{32}S$^-$/^{28}Si$^-$ ratios obtained during isotope analyses. A S$^-$/Si$^-$ sensitivity factor of 3.0 was used to calculate S concentrations. In lack of a SiC standard with known S content, the S$^-$/Si$^-$ sensitivity factor was inferred from ion yields obtained for Si$^-$ in synthetic SiC and S$^-$ in Mundrabilla FeS (Hoppe et al. 2012).

Magnesium and Ca abundances were measured in a separate series by rastering a 1–2 pA O$^-$ primary ion beam (16 keV energy, ~200 nm size) over 13 MS grains

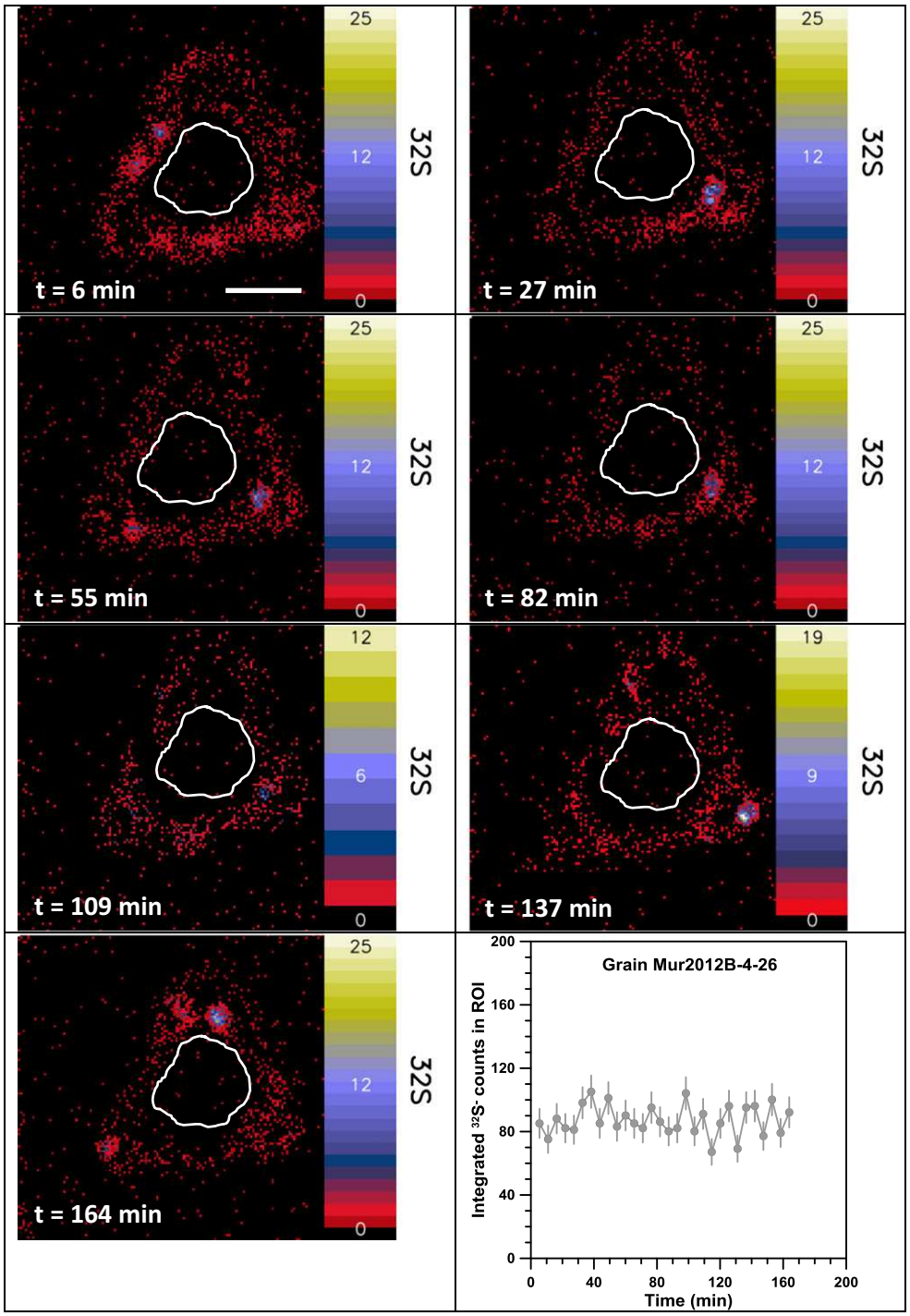

Fig. 2. NanoSIMS ion images of $^{32}S^-$ for grain #26 at six different times. The plot in the lower right shows the integrated $^{32}S^-$ ion signal for the region of interest (ROI) outlined in each panel and in Fig. 1 as a function of time. While the $^{32}S^-$ intensity stays stable within the ROI, it varies with time at the grain boundary. Scale bar in the upper left image is 1 μm and applies to all ion images.

measured for S (one MS grain measured for S could not be relocalized). Raster sizes were similar to those used for the S isotope measurements. Prior to the Mg and Ca abundance measurements, an intense primary ion beam (~400 pA for 2–3 min and raster size somewhat larger than the grain size) was used for cleaning and O

implantation to increase secondary ion yields. Magnesium and Ca (and Al) abundances were measured by recording high-resolution ion images of $^{24}Mg^+$, $^{27}Al^+$, $^{28}Si^+$, and $^{40}Ca^+$ in multicollection mode (256 × 256 pixels, total integration time ~55–65 min grain^{-1}, divided into 5–6 image planes). All species were measured with an entrance slit width of 30 μm and exit slit widths of 80 μm which permits us to separate all relevant isobaric interferences, especially $^{12}C_2$ and $^{12}C^{28}Si$.

In the absence of a SiC standard with known Mg and Ca concentrations, Mg^+/Si^+ and Ca^+/Si^+ sensitivity factors ε were determined on NIST SRM611 glass ([Mg] = 432 ppm, [CaO] = 11.4 wt%; Jochum et al. 2011), which gave $\varepsilon(Mg^+)/\varepsilon(Si^+) = 3.3$ and $\varepsilon(Ca^+)/\varepsilon(Si^+) = 4$. Because of matrix and topographic effects these sensitivity factors may not be strictly valid for SiC. Sensitivity factors for Mg^+/Si^+ and Ca^+/Si^+ inferred from ion yields obtained for Si^+ in SiC, Mg^+ in spinel, and Ca^+ in perovskite are about a factor of two higher. Thus, an estimated uncertainty of a factor of two should be considered for all inferred element/Si ratios.

RESULTS

Carbon- and Silicon-Isotopic Compositions

The 23 presolar SiC grains of this study have $^{12}C/^{13}C$ ratios between 3.0 and 134, $\delta^{29}Si$ values from −37 to +142‰ and $\delta^{30}Si$ values from −13 to +118‰, well within the known ranges of presolar SiC (Zinner 2014). In the Si-three-isotope diagram, they plot along the MS line, with a few outliers slightly shifted to the ^{30}Si-rich side (Fig. 3). Among the studied 23 grains are 1 AB grain, 19 MS grains, and 3 Y grains.

Sulfur-Isotopic Compositions and Abundances

From the 19 MS grains we selected 14 for S isotope studies. The remaining 5 MS grains were not measured because two of them could not be relocated, two had comparatively low Si ion intensities due to topographic effects, and one showed a very rough surface texture. Figure 1 shows $^{28}Si^-$ and $^{32}S^-$ ion images integrated over all planes, and SEM photographs of the 14 MS grains analyzed. The $^{32}S^-$ ion images reveal that great care must be taken when selecting areas for S data reduction. Many of the concentration hotspots and the increased S abundances along grain boundaries and texture lines within grains are likely caused by contamination and must be excluded for the data reduction. We cannot fully rule out that some of the hotspots are from natural CaS or other sulfide inclusions. However, to treat our data in a conservative way, these hotspots, which have normal S isotope compositions, will not be considered here.

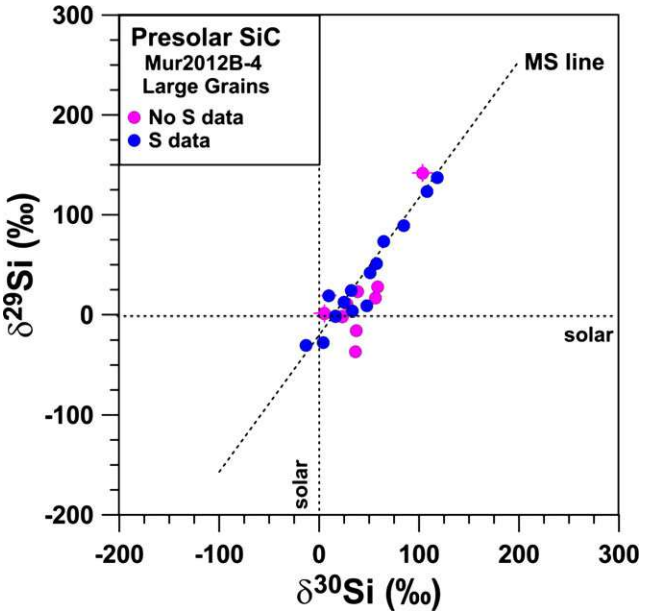

Fig. 3. Silicon-isotopic compositions, given as per mil deviation from the solar $^{29}Si/^{28}Si$ and $^{30}Si/^{28}Si$ ratios, of 23 presolar SiC grains from Murchison sample Mur2012B-4. Errors are 1σ. All grains plot along the SiC MS line (Zinner et al. 2007), with a few outliers to the ^{30}Si-rich side. Grains shown in blue (see Web version of this article), all of which are of the MS type, were subsequently studied for S-isotopic compositions.

Abundances and isotopic compositions for the 14 grains studied are given in Table 1. The CI chondrite-normalized S/Si ratios[4] are between 1.9×10^{-5} and 1.9×10^{-4}, if we exclude grains Mur2012B-4-48, Mur2012B-4-50, Mur2012B-4-33, and Mur2012B-4-47. The first two grains have very high (S/Si)/CI ratios of 1.0×10^{-2} and 6.6×10^{-3}, respectively. A comparison of $^{32}S^-$ ion images with the corresponding surface textures seen in the SEM images strongly suggest that S is dominated by contamination everywhere in these two grains. Their normal S-isotopic compositions (Table 1) are compatible with this view.

The other two grains excluded have relatively low (S/Si)/CI ratios of 3.3×10^{-4} and 4.9×10^{-4}, but again large patches of S contamination on the grains may have compromised the S isotope and abundance data. In the following we focus on the 10 MS grains for which contamination, if any, is a minor possibility on sufficiently large grain areas (see outlines in Fig. 1) and assume that their S data represent mainly intrinsic S. The two line profiles of $^{32}S^-$ intensities shown in the two

[4]Henceforth we write (S/Si)/CI for CI chondrite-normalized values, which is also equivalent to solar-normalized.

Table 1. C-, Si-, and S-isotopic compositions, and atomic and CI-normalized S/Si ratios of presolar SiC mainstream grains from Murchison.

Grain no. Mur2012B-4-	Size (μm)	$^{12}C/^{13}C$	$\delta^{29}Si$ (‰)	$\delta^{30}Si$ (‰)	$\delta^{33}S$ (‰)	$\delta^{34}S$ (‰)	Low S area[a]	S/Si[e] (10^{-5})	(S/Si)/CI (10^{-4})
6	1.4	79.1 ± 0.3	4 ± 2	33 ± 3	205 ± 227	172 ± 96	0.24	2.41	0.540
8	1.8	67.5 ± 0.2	13 ± 2	25 ± 3	124 ± 203	1 ± 82	0.06	7.59	1.70
9	3.3	48.4 ± 0.1	−30 ± 2	−13 ± 2	−106 ± 156	−59 ± 68	0.04	8.62	1.93
10	2.5	81.7 ± 0.3	9 ± 2	48 ± 2	−91 ± 98	−10 ± 44	0.48	4.30	0.963
19[b]	2.4 × 1.1	48.5 ± 0.2	124 ± 2	108 ± 3		79 ± 135	0.20	4.73	1.06
26	2.0	29.6 ± 0.0	137 ± 1	118 ± 2	−253 ± 191	−85 ± 92	0.29	0.947	0.212
30	1.4	41.5 ± 0.1	89 ± 2	85 ± 3	−124 ± 448	−78 ± 197	0.16	0.851	0.190
33[c]	1.7	63.5 ± 0.2	51 ± 2	57 ± 2	3 ± 121	−5 ± 52	0.06	22.0	4.92
35	1.4	66.3 ± 0.2	−27 ± 2	4 ± 2	−253 ± 202	−134 ± 94	0.23	1.91	0.427
36	2.4	51.8 ± 0.2	42 ± 2	51 ± 2	634 ± 478	276 ± 179	0.08	1.17	0.261
47[c]	2.1 × 1.6	58.8 ± 0.5	19 ± 6	10 ± 7	−151 ± 165	22 ± 78	0.10	14.8	3.31
48[d]	6.6 × 5.7	54.0 ± 0.3	24 ± 5	32 ± 6	−35 ± 29	−10 ± 13		447	100
50[d]	3.1 × 2.1	48.1 ± 0.1	−1 ± 2	16 ± 2	−5 ± 19	−7 ± 8		288	64.4
51	3.5 × 2.6	56.0 ± 0.2	73 ± 2	65 ± 2	73 ± 130	68 ± 56	0.16	4.17	0.933

[a]Fraction of grain area used for S data reduction.
[b]No reliable ^{33}S data.
[c]Possibly moderate contributions from S contamination.
[d]Probably high S contamination due to rough surface texture.
[e]Absolute S abundances in ppm wt. can be calculated by multiplying S/Si ratios by 8.00×10^5.

lowest panels of Fig. 1 and the depth profile of $^{32}S^-$ intensities shown in Fig. 2 support this view. We integrated over these grain regions with low and homogeneous S abundances to find $\delta^{33}S$ values between -253 ± 191‰ and $+634 \pm 478$‰ and $\delta^{34}S$ values between -134 ± 94‰ and $+276 \pm 179$‰. The S-isotopic compositions of all grains agree with the terrestrial composition (solar) within 2σ. The large uncertainties arise from the very low S abundances. In the S three isotope diagram the grain data plot along a line with slope of ~1.8 (Fig. 4) which, however, has only moderate statistical significance (confidence level of 86% for a slope >1). We note that the literature data for the interstellar medium (ISM) and the carbon star IRC+10 216 plot closely to the fit line resulting from our measurements.

There is no apparent correlation between the S-isotopic composition and Si-isotopic composition (Fig. 5), $^{12}C/^{13}C$ (Fig. 6), or S elemental abundance (Fig. 7). The means (calculated by integrating the secondary ion counts from all grains of interest) of the 10 grains (excluding Mur2012B-4-33/47/48/50 as stated earlier) are $\delta^{33}S = -8 \pm 56$‰ and $\delta^{34}S = 13 \pm 23$‰. These values are compatible with the solar (or chondritic) S-isotopic composition.

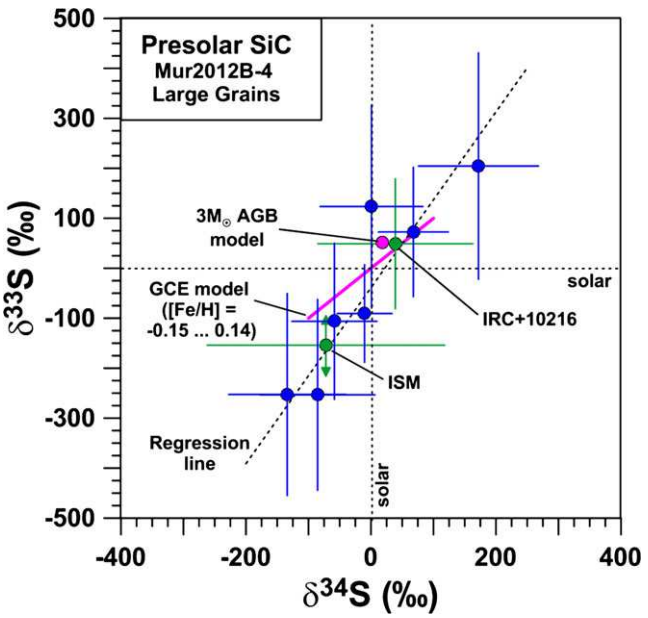

Fig. 4. Sulfur-isotopic compositions, given as per mil deviation from the solar $^{33}S/^{32}S$ and $^{34}S/^{32}S$ ratios, of seven presolar SiC mainstream grains from Murchison sample Mur2012B-4. Errors are 1σ. Two SiC grains with error >400‰ in $\delta^{33}S$ and one grain for which only $\delta^{34}S$ data exist are not shown. The regression line through the SiC data points is given by $\delta^{33}S = (1.8 \pm 0.7) \times \delta^{34}S - (39 \pm 57)$. Predictions for a 3 $M_\odot$ AGB star of solar metallicity (Cristallo et al. 2009) and from a GCE model (Kobayashi et al. 2011), adjusted to go through solar and extrapolated to higher than solar metallicities ([Fe/H] = 0.14), as well as astronomical observations of carbon star IRC + 10216 and the ISM (Mauersberger et al. 2004) are shown for comparison.

Magnesium and Calcium Abundances

The Mg and Ca abundance data are given in Table 2 as atomic ratios relative to Si. The Mg and Ca

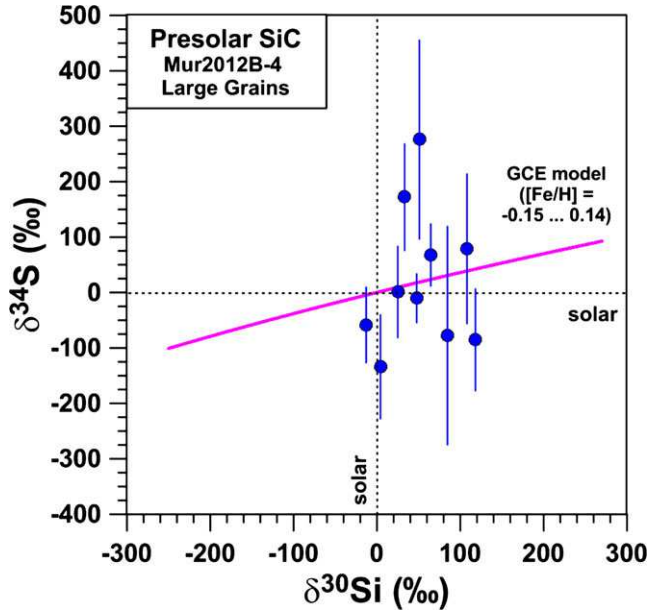

Fig. 5. $\delta^{34}S$ as function of $\delta^{30}Si$ of 10 presolar SiC MS grains from Murchison sample Mur2012B-4. Errors are 1σ. Predictions from the GCE model of Kobayashi et al. (2011), adjusted to go through solar and extrapolated to higher than solar metallicities ([Fe/H] = 0.15), are shown for comparison.

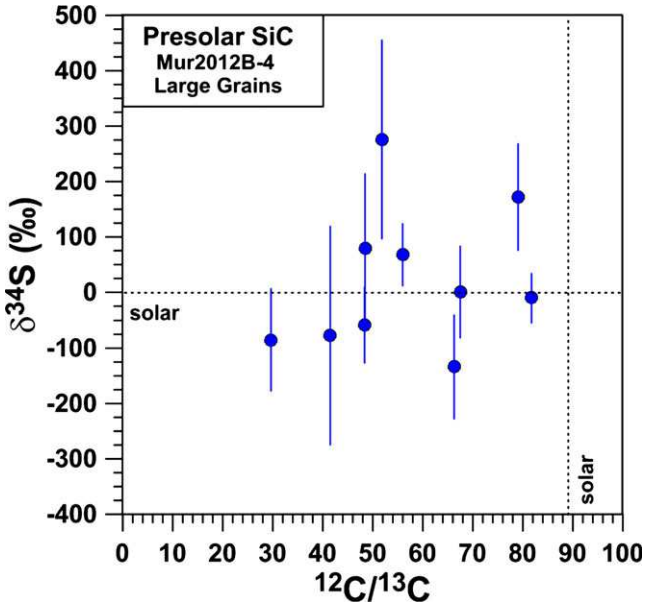

Fig. 6. $\delta^{34}S$ as function of $^{12}C/^{13}C$ of 10 presolar SiC mainstream grains from Murchison sample Mur2012B-4. Errors are 1σ.

ion images indicate variable degrees of contamination and only low Ca areas were considered for the data reduction. Because the spatial resolution is worse than for the S measurements, selected areas are generally smaller than those of the S data reduction (cf. grain Mur2012B-4-26 in Figs. 1, 2, and 8). The Ca and Mg in grains Mur2012B-4-48, Mur2012B-4-50, and Mur2012B-4-8 are dominated by contamination. Because the S abundances of the grains Mur2012B-4-33 and Mur2012B-4-47 are questionable and the S contamination-free area in grain Mur2012B-4-9 very small, we will not use the Mg and Ca data of these three grains. Grain Mur2012B-4-19 could not be measured for Mg and Ca because it was lost. The remaining seven grains have atomic Mg/Si ratios between 1.4×10^{-5} and 5.3×10^{-5} and Ca/Si ratios between 4.0×10^{-5} and 5.5×10^{-4}.

All of the measurements shown in Fig. 9 (left) yield larger Mg/Si ratios than would be expected from the corresponding S/Si ratios for the grains for stoichiometric MgS incorporated into SiC. The line in Fig. 9 shows where Mg/Si: S/Si = 1:1. Overall, there is some correlation of the Mg/Si ratios with S/Si ratios, and a fit forced to go through the origin gives a slope slightly larger than unity (Fig. 9, left). Given the uncertainties in sensitivity factors due to matrix and topographic effects, the observed Mg/Si versus S/Si correlation is compatible with a slope of 1. However, we note that four of the grains (#10, 30, 35, 51) plot closely along a parallel line above the 1:1 line which suggests a Mg "excess" (for S/Si = 0). Thus, Mg might have been incorporated into SiC as MgS and MgX, where X is another charge-balancing element (possibly C).

The Ca/Si ratios do not correlate with corresponding S/Si ratios (Fig. 9, right). On average, the Ca abundances are higher by a factor of about 10 (Fig. 9, right). Assuming that these data are not dominated by contamination and that they largely reflect the true amounts of Ca condensed into SiC, the amounts of S are far too low to explain the origin of Ca from incorporated CaS. These findings are discussed below.

DISCUSSION

Sulfur Nucleosynthesis

Sulfur is produced mainly in massive stars by charged particle reactions during hydrostatic and explosive nuclear burning stages, whereas contributions from low and intermediate stars are small (Timmes et al. 1995). Sulfur-isotopic compositions vary significantly in the interior of massive stars due to different production mechanisms in different layers. For example, in the 15 $M_\odot$ Type II SN model from Rauscher et al. (2002), $\delta^{34}S$ varies between −880‰ in the interior Si/S zone, >5000‰ in the intermediate

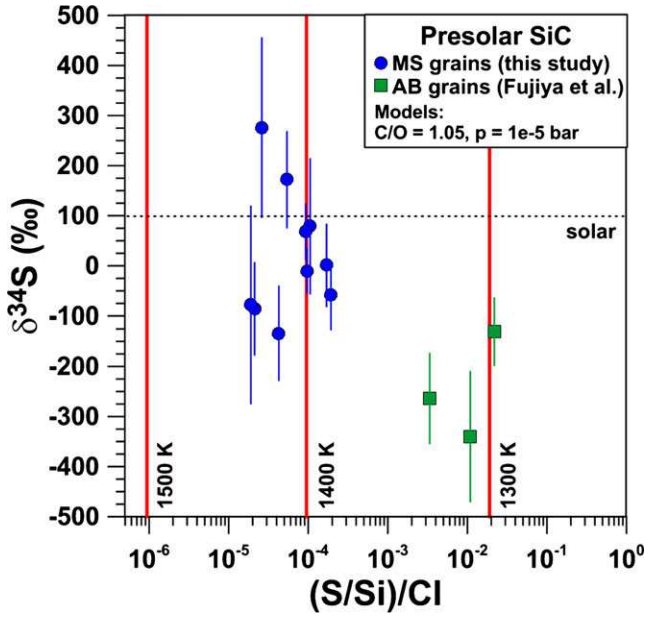

Fig. 7. $\delta^{34}S$ as function of CI-normalized S/Si ratios of 10 presolar SiC mainstream grains from Murchison sample Mur2012B-4 (circles). Errors are 1σ. Data for three AB grains with ^{32}S excesses (squares; Fujiya et al. 2013) are shown for comparison. Predictions for CI-normalized S/Si ratios in SiC from equilibrium condensation calculations with C/O = 1.05 and total pressure of 10^{-5} bar are indicated for three different temperatures by vertical lines, assuming solid solution of CaS (major) and MgS (minor) in SiC.

O-rich zones, and ~0‰ in the outer He- and H-rich zones. Presolar SiC grains from Type II SNe (the C and X grains) have strong excesses in ^{32}S (Gyngard et al. 2010; Hoppe et al. 2012; Xu et al. 2012). The X grains may have the signature of S from the Si/S burning zone (Hoppe et al. 2012). The much larger ^{32}S excesses in type C grains are best explained by incorporation of radioactive ^{32}Si into the SiC structure, followed by in situ decay to ^{32}S (Pignatari et al. 2013). Silicon-32 is produced by neutron capture at high neutron densities and a possible site in the Rauscher et al. (2002) model is the outer layer of the O/C zone. This zone is rich in ^{32}Si and has overabundances of $^{29,30}Si$, as observed in C grains. Similarly, the smaller ^{32}S enrichments observed in some AB grains can be explained by incorporation of ^{32}Si which is expected to be produced in significant amounts in born-again AGB stars (Fujiya et al. 2013), along with low $^{12}C/^{13}C$ ratios as observed in AB grains.

We note that all scenarios explaining ^{32}S excesses from in situ decay require very fast cooling of the stellar ejecta and fast condensation for incorporation of ^{32}Si into SiC with timescales of the same magnitude as the ^{32}Si half-life (153 yr).

Table 2. Mg, Al, and Ca abundances (atomic ratios relative to Si) of presolar SiC mainstream grains from Murchison.

Grain no. Mur2012B-4-	Mg/Si[e] (10^{-5})	Al/Si[e] (10^{-2})	Ca/Si (10^{-4})
6	2.79	2.81	2.40
8[a]	298	2.14	309
9[b]	29.5	0.262	14.9
10	5.23	0.059	3.58
19[c]	n.m.	n.m.	n.m.
26	1.25	0.405	0.64
30	2.29	0.046	1.30
33[d]	43.0	4.46	26.2
35	3.26	2.66	5.50
36	1.41	3.22	0.40
47[d]	24.5	0.075	20.6
48[a]	278	4.05	179
50[a]	194	7.85	175
51	5.28	0.0049	1.74

[a]Strong contributions from Mg and Ca contamination.
[b]Very small S contamination-free area.
[c]n.m.: not measured; grain was lost prior to Mg-Al-Ca measurement.
[d]Possibly moderate contribution from Mg and Ca contamination.
[e]Absolute Mg, Al, and Ca abundances in ppm wt. can be calculated by multiplying Si-normalized elemental ratios by 6.06×10^5 (Mg), 6.73×10^5 (Al), and 1.00×10^5 (Ca), respectively.

The "normal" AGB stars are not significant producers of elemental S, and their surface abundances of heavy S isotopes only mildly increases with time during the third dredge-up episodes. Unlike born-again AGB stars, the AGB parent stars of the MS grains only produce tiny amounts of ^{32}Si (Cristallo et al. 2009). The enrichments in the heavy S isotopes from slow neutron capture are predicted to be small. The 1.5 and 3 $M_\odot$ solar metallicity AGB star models of Cristallo et al. (2009) (see also http://fruity.oa-teramo.inaf.it/), which can be considered representative of the most likely stellar sources of MS grains, predict $\delta^{33}S = +10‰$ and $\delta^{34}S = +7‰$ (1.5 $M_\odot$), and $\delta^{33}S = +51‰$ and $\delta^{34}S = +18‰$ (3 $M_\odot$) after the final pulse. Subsolar metallicity yield somewhat higher enrichments in ^{33}S and ^{34}S, e.g., for $Z/Z_\odot = 0.43$, $\delta^{33}S = +20‰$ and $\delta^{34}S = +14‰$ for a 1.5 $M_\odot$ AGB star, and $\delta^{33}S = +66‰$ and $\delta^{34}S = +42‰$ for a 3 $M_\odot$ AGB star (Cristallo et al. 2009).

The expectation that the surface enrichments in ^{33}S and ^{34}S remain small during evolution of low- and intermediate-mass stars is supported by one measurement for the carbon star IRC+10216 which has $\delta^{33}S = +49 \pm 130‰$ and $\delta^{34}S = +39 \pm 124‰$ (Mauersberger et al. 2004). The large uncertainties of S-isotopic compositions in individual SiC MS grains from this study of around 50–100‰ for $\delta^{34}S$ (Table 1) make a meaningful comparison with model predictions

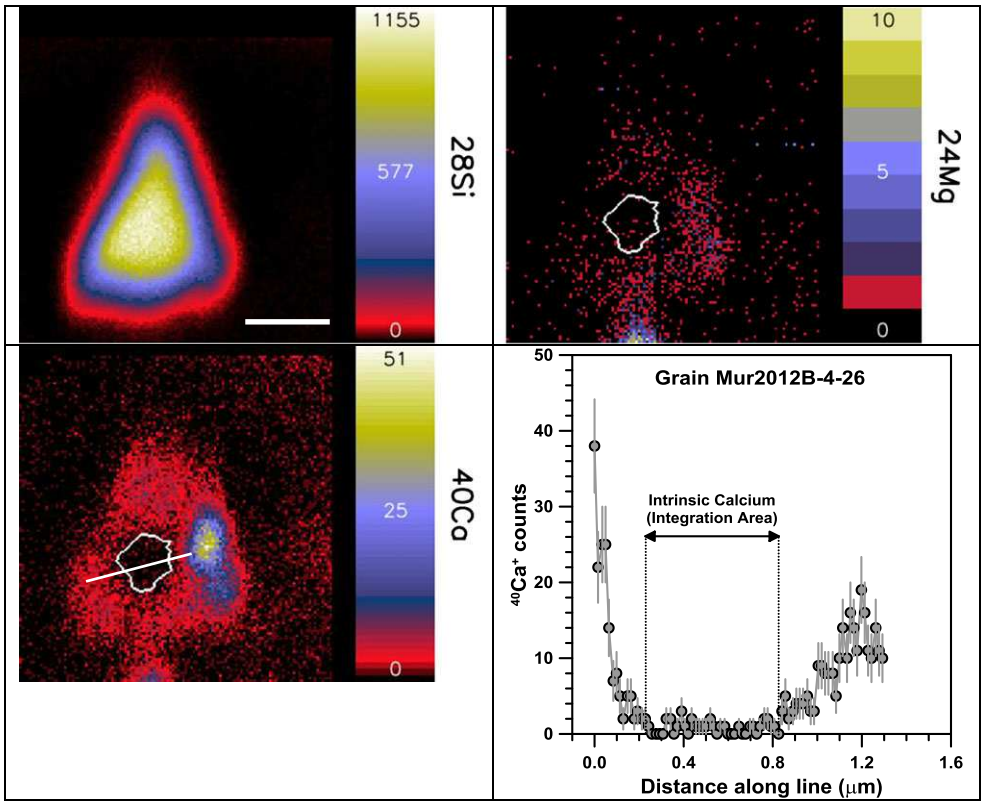

Fig. 8. NanoSIMS ion images of $^{28}Si^+$, $^{24}Mg^+$, and $^{40}Ca^+$ for SiC MS grain Mur2012B-4-26. The scale bar in the upper left image is 1 μm and applies to all ion images. Color scale (white-yellow-blue-red-black; see Web version of this article): White represents the maximum in each image and black the minimum. The white outlines in the ^{24}Mg and ^{40}Ca ion images show the area assumed to be largely free of Ca contamination. The panel in the lower right shows the profile of ^{40}Ca along the line drawn in the respective ion image. Each point in the line profile represents a superposition of 2 × 2 pixels. The two vertical lines show the intersection with the outline of the low Ca area.

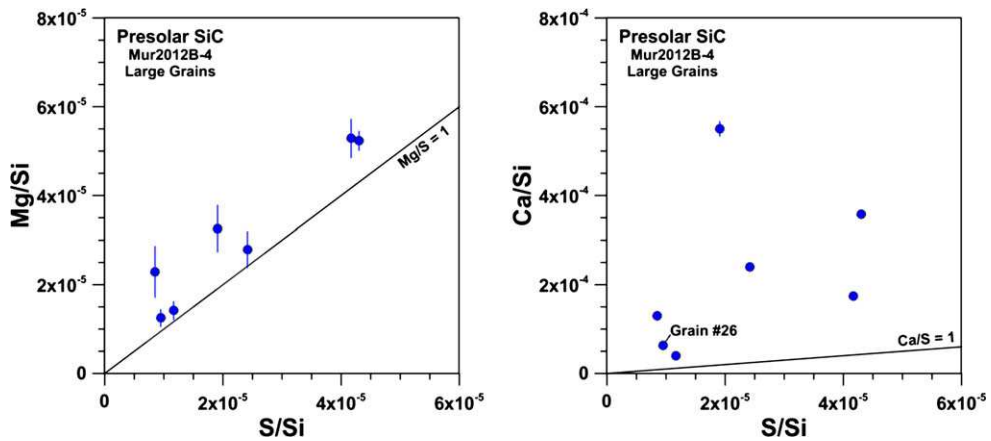

Fig. 9. Mg/Si versus S/Si (left) and Ca/Si versus S/Si (right) in micrometer-sized MS grains from Murchison sample Mur2012B-4. Errors are 1σ. The solid lines represent Mg/S = 1 and Ca/Si = 1, respectively.

difficult. The means of $\delta^{33}S = -8 \pm 56‰$ and $\delta^{34}S = +13 \pm 23‰$ of our SiC grains are at least qualitatively consistent with only small enrichments in ^{33}S and ^{34}S in the parent stars' stellar envelopes.

Galactic Chemical Evolution (GCE)

The Si-isotopic compositions of MS grains plot along a line given as $\delta^{29}Si = 1.37 \times \delta^{30}Si - 20$ (Zinner

et al. 2007), with δ^{30}Si values between −50 and +150‰. This line is thought to represent a range of initial Si compositions of the parent stars of MS grains. This range reflects the different composition of the ISM from which the stars originated. Thus, the range was established by GCE. The Si-isotopic compositions are not strongly affected by AGB star nucleosynthesis and are not expected to change by more than 4% during the lives of solar metallicity AGB stars with masses of about 1.5–3 $M_{\odot}$ (Zinner et al. 2006).

The S-isotopic compositions are also expected to only change by several percent in AGB stars. Some GCE models predict increasing $^{33,34}S/^{32}S$ and $^{29,30}Si$ with increasing metallicity (Kobayashi et al. 2011) and both δ^{29}Si versus δ^{30}Si and δ^{33}S versus δ^{34}S should evolve along a line with slope about unity for metallicities of [Fe/H] > −0.5. However, changes in δ^{30}Si will be ~2.7× larger than those in δ^{34}S. Thus, the 200‰ variation in δ^{30}Si observed for MS grains should be accompanied by only a 70‰ variation in δ^{34}S.

In a δ^{33}S versus δ^{34}S diagram, the MS grains of this study plot along a line with slope 1.8 ± 0.7, in rough agreement with the results from the GCE model of Kobayashi et al. (2011) (Fig. 4). Interestingly, the S-isotopic compositions measured for the ISM and for the carbon star IRC+10216 (Mauersberger et al. 2004) also follow this trend, yet with large measurement uncertainties. The SiC grains of this study have Si-isotopic compositions with δ^{30}Si values between −13‰ and +118‰, and they almost cover the full range of δ^{30}Si values observed for MS grains. Considering our analytical uncertainties we cannot detect the predicted 50‰ variation in δ^{34}S (inferred from the 130‰ variation in δ^{30}Si) from the Kobayashi et al. (2011) model and we find that our δ^{34}S and δ^{30}Si values are uncorrelated (Fig. 5). Although the apparent δ^{33}S versus δ^{34}S correlation looks promising, the low S abundances with their large uncertainties in S-isotopic compositions make meaningful conclusions about the initial S-isotopic compositions of the MS grains parent stars' difficult.

Sulfur Chemistry and Dust Formation around AGB Stars

We now discuss the incorporation of S into the MS grains. The observed abundance variation by a factor of 10 (Fig. 7) is compatible with what is observed for other elements contained in SiC MS grains (Amari et al. 1995), and such variations are expected from fractional condensation in the circumstellar shells. Equilibrium condensation calculations for the atmosphere of AGB stars can reproduce the element patterns in SiC for C/O = 1.05, total $P = 10^{-5}$ bar and T = 1200–1350 K (Lodders and Fegley 1995). Taking the same values for C/O and total P, and considering solid solution of CaS and MgS in SiC, the observed S abundances in MS grains can be reproduced at $T \sim 1400$ K (Fig. 7), about 50–200 K higher than inferred for other elements. At $T = 1300$ K the calculated S abundances from CaS incorporation, which is expected to dominate over MgS, are more than two orders of magnitude higher than observed (Fig. 7). Our calculations assume ideal solid solution of CaS and MgS in SiC; and that these sulfides do not form separate pure phases. If the solution is not ideal, the calculated amounts of CaS (and MgS) are too high and predicted S/Si ratios represent only upper limits; the same holds if CaS (and MgS) condense separately from SiC. The comparison of our data with the condensation calculations indicates that ideal solution of CaS into SiC does not apply, that separate formation of CaS occurred, or both.

Lodders and Fegley (1995) and Hoppe et al. (2001) discussed the conditions favoring ideal solid solution in SiC. The atomic radii and crystal structures of dissolving compounds provide a good first-order guide. In Lodders and Fegley (1995), the thermochemical stability (activity) of CaS and its similar crystal structure to SiC was used as criteria for selecting CaS for solid solution in SiC. The ionic radius of Ca (1.2 Å for 8-coordinated Ca) is only slightly larger than the radius of covalent Si (1.17 Å), and substitution of Si by Ca seems possible. However, the substitution of C (covalent 0.77 Å) by S^{2-} (1.72 Å) in the lattice does not match well, and ideal solid solution of large quantities CaS in SiC is unlikely. Hynes et al. (2010, 2011) identified five CaS subgrains in a microtome slice of a SiC type AB grain that are compositionally consistent with CaS as indicated by EDXS and microdiffraction. The authors suggested that these subgrains resulted from exsolution of CaS that condensed in solid solution with the SiC, which would contradict our conclusions. However, we want to point out that it is also possible that CaS condensed as a "pure" separate phase that was captured by the growing SiC grains.

We found that Ca is about 10 times more abundant than S in the grains (see earlier section), and another charge-balancing element other than S is needed. The most likely candidate for this is CaC_2, based on its stability (expressed by thermochemical activity) in AGB shells. The stability of CaC_2 closely follows that of CaS under the P–T and C/O conditions considered here. There is some uncertainty in the thermodynamic properties of these Ca compounds. A recent assessment of the Ca-C-O-S system by Lindberg and Chartrand (2009) suggests different stabilities for CaS and CaC_2 than evaluated in earlier compilations. Using their assessed thermodynamic data, we find activities of CaC_2 very similar to those of CaS in the circumstellar

envelopes (CSEs). The CaC_2 stability is particularly favored if conditions in the CSE also lead to stable graphite (activity of C is unity). In addition, Lindberg and Chartrand (2009) describe the complete miscibility in the solid solution between CaS and the cubic high temperature modification of CaC_2, and that this solid solution exhibits the cubic rock salt structure. Thus, Ca can condense as both, CaS and CaC_2, and very likely as Ca(S, C_2) solid solution series into SiC, depending on the details of P, T, and C/O conditions.

There could also be some significant contributions from unrecognized Ca contamination, which complicates the interpretation of the Ca and S abundances. But, at least for grain Mur2012B-4-26, this possibility appears unlikely as we found a relatively large area with low and homogeneous Ca content (Fig. 8). This remains true even if we consider the estimated uncertainties of a factor of two to three on the Ca/S quantification due to matrix and topographic effects.

The observed correlation between Mg and S abundances (Fig. 9, left) suggests MgS solid solution in SiC instead of CaS. The rock-salt structured MgS is also favorable for solid solution in SiC. The ionic radius of Mg (0.80 Å) is smaller than the covalent radius of atomic Si, and replacement of Si by Mg should proceed more easily than the Ca for Si substitution. As above for Ca, the ionic radius of S^{2-} is larger than the covalent radius of C and not favorable but overall the situation seems more favorable for MgS solid solution than for CaS. MgS is generally less refractory than CaS (or CaC_2) and lower temperatures are required to condense the same amounts of S into SiC from MgS than CaS. Thus, the much lower Mg than Ca abundance in the grains is not surprising although Mg is almost 20 times more abundant than Ca in solar composition. The much higher Ca than S abundance and the Mg-S correlation suggests that S entered SiC as MgS. As done above for Ca, Mg carbides must also be considered. Not too much is known about Mg carbides, but there seem to be two meta-stable carbides Mg_2C_3 and MgC_2, and a metastable Mg_5C_{70} fulleride (Chen and Schmid-Fetzer 2012). These authors also recommend using the thermodynamic properties from the JANAF tables for the lower carbides, which we had been using before. We find that Mg carbides are significantly less stable than MgS, and that there is no similarity in carbide and sulfide stability as seen for Ca compounds. Thus, we can be relatively certain that MgS is the major compound responsible for incorporating Mg into SiC.

The amount of S calculated to condense into SiC, assuming incorporation of CaS and MgS, is shown for three temperatures in Fig. 7. These values are fairly high, and are dominated by contribution of S from CaS. The calculated amounts of S from MgS condensation alone are rather small, e.g., the CI chondrite-normalized S/Si ratio is about 1.4×10^{-5} at 1200 K, and about 1×10^{-7} at 1300 K. These values are lower than observed for SiC grains in Fig. 7. In the absence of activity data for Ca and Mg carbides and sulfides in SiC, and the uncertainty if other sulfides (e.g., of Fe, Ni, or other more abundant transition metals) contribute S, it is difficult to draw more conclusions here except that calculated amounts of condensed S from MgS incorporation reflect firm lower limits, and amounts calculated from CaS condensation are very likely overestimated.

Implications for SiC Type AB Grains

The AB grains with ^{32}S excesses have ~100× higher S abundances than the MS grains of this study (Fig. 7). It has been assumed by Fujiya et al. (2013) that S in these grains is dominated by contamination (their small sizes did not allow for an extensive cleaning before analysis). However, at least 25% of S must be nonsolar S to account for the observed isotope anomalies, which corresponds to (S/Si)/CI of a few times 10^{-3}, which is still almost two orders of magnitude higher than in MS grains. It can be seen from Fig. 7 that predicted S/Si ratios in SiC from AGB stars strongly depend on T. For C/O = 1.05, $p = 10^{-5}$ bar, and $T = 1300$ K it is in principle possible to match the S abundances of AB grains with ^{32}S excesses if ideal solid solution of CaS in SiC occurred. However, if we assume that conditions for condensation around born-again AGB stars are comparable to those around AGB stars that donated the MS grains, then the 100× higher S abundance in AB grains is hard to understand without invoking in situ decay of ^{32}Si decay. This is especially true considering that the observed S abundance and S/Si ratio in Sakurai's object are subsolar (Asplund et al. 1999). Therefore, the low S abundances of MS grains support the notion that the isotopically light S in AB grains is a mixture of radiogenic ^{32}S (from in situ ^{32}Si decay after formation of SiC with $^{32}Si/^{28}Si \sim 10^{-3}$) and isotopically normal S, mostly contamination.

A critical question that must be addressed is whether the conditions for SiC formation around born-again AGB stars are indeed comparable to those around normal AGB stars. Born-again AGB stars evolve much more rapidly than normal AGB stars, on a time scale of months (Asplund et al. 1999): From April 1996 to October 1996 the effective temperature T_{eff} of Sakurai's object decreased by almost 1000 K to a value of ~7000 K. In 1998 T_{eff} had reached ~5000–6000 K, still significantly higher than in carbon stars (Lodders and Fegley [1995] and references therein). The mass loss

rate (dM/dt) increased drastically over time to a few times 10^{-6} $M_{\odot}$ yr^{-1} in 1999 when Sakurai's object developed a thick dust shell, mostly graphitic carbon, with an inner shell temperature of ~1250 K (Tyne et al. 2002). The mass loss rate is at the upper end of what is observed for carbon stars (Olofsson et al. 1990) and the surface C/O ratio of 2.5 (Asplund et al. 1999) higher than the mean value of ~1.15 observed for cooler N- and J-type carbon stars (Lodders and Fegley [1995] and references therein). From the work of Lodders and Fegley (1995), it is evident that the SiC condensation temperature depends only marginally on the C/O ratio and essentially no changes are expected for predicted S abundances for higher C/O ratios. Whether conditions as observed in Sakurai's object are in favor of equilibrium condensation of SiC with total pressure and temperature as inferred for the parent stars of MS grains is hard to tell but it appears entirely possible. This needs to be explored in more detail, in conjunction with more data analysis to put models on a firm analytical base.

We are facing a different situation if conditions around born-again AGB stars favor the separate condensation of sulfides, e.g., CaS, and their incorporation into SiC grains, as observed in one AB grain (Hynes et al. 2010, 2011). In this case, S abundances could be much higher than calculated for equilibrium condensation. If we assume that production of ^{32}Si in born-again AGB stars is much lower than predicted, then S-isotopic compositions are expected to show imprints of GCE and S nucleosynthesis. Like in normal AGB stars, nucleosynthesis in born-again AGB stars is expected to enrich ^{33}S and ^{34}S due to neutron capture reactions on ^{32}S. If the surface enrichment in these two isotopes remains small then GCE effects might dominate. From the S isotope data of our MS grains (Fig. 4) we cannot completely rule out that the enrichments in ^{32}S of 25% are the fingerprint of GCE, which, however, appears unlikely in the context of the GCE model by Kobayashi et al. (2011). Nevertheless, more work is needed to unequivocally unravel the origin of ^{32}S excesses in AB grains. What would be helpful in this respect would be the finding of AB grains with ^{32}S excesses of 50% or more, which would substantiate the proposed radiogenic origin.

SUMMARY AND CONCLUSIONS

1. We have analyzed 14 presolar SiC MS grains for C-, Si-, and S-isotopic compositions and S elemental abundances. For 10 grains contamination with S of laboratory or meteoritic origin appears to be low. These grains have (S/Si)/CI ratios from 2×10^{-5} to 2×10^{-4}. All grains have S-isotopic compositions compatible with solar within 2σ, with mean values of $\delta^{33}S = -8 \pm 56‰$ and $\delta^{34}S = 13 \pm 23‰$. In a $\delta^{33}S$ versus $\delta^{34}S$ representation the data plot along a line with slope 1.8 ± 0.7.
2. The mean S isotope composition of our relatively small presolar SiC MS grain sample deviates by at most a few percent from solar. This is consistent with astronomical observations of carbon star IRC+10216 and the ISM as well as with model predictions of low-mass AGB stars.
3. The observed correlation between $\delta^{33}S$ and $\delta^{34}S$ in SiC MS grains may be an imprint of GCE, and not local stellar nucleosynthesis. However, large errors due to the low S abundances prevent meaningful conclusions with respect to the initial S-isotopic compositions of the parent stars of MS grains.
4. Assuming CaS and MgS solid solution in the MS SiC grains, the observed low S abundances are lower than predicted from equilibrium condensation calculations at conditions (C/O = 1.05, p = 10^{-5} bar, T = 1200–1350 K) at which the abundances of other, more refractory elements can be matched. This indicates that ideal solid solution of CaS in SiC does not apply, that separate formation of CaS occurred, or both. The condensation of CaC_2 is likely to compete with that of CaS. The correlation between Mg and S abundances in MS grains suggests solid solution of MgS in SiC, but calculated abundances only assuming MgS are too low. MgS condensation yields lower limits for the amount of S condensed, whereas CaS condensation likely overestimates values. In absence of thermodynamic activity data, no more firm conclusions can be drawn at this time.
5. The low abundances of S in MS grains lend support to the model that the significantly higher abundances of ^{32}S-rich sulfur in some AB SiC grains are the result of in situ decay of radioactive ^{32}Si, which is predicted to be produced in large quantities in born-again AGB stars, the likely sources of some fraction of AB grains. The observations of CaS subgrains in AB grains (Hynes et al. 2010, 2011), but not MS grains here, could also plausibly explain the two orders of magnitude higher S abundances in the AB grains. If CaS subgrains (and possibly MgS and other sulfides) were incorporated into the growing AB grains, one may not need to invoke in situ ^{32}Si decay to explain the larger S abundances. However, in this case it is not explained why only the AB grains show such large excesses of ^{32}S of about 25%, and how GCE would only affect AB stellar sources that way. We also note that the different chemistries of the AB

and MS grains may point to different chemical environments in the circumstellar envelopes, which need to be explored more, in conjunction with more data analysis to put models on a firm analytical base.

Acknowledgments—We thank Antje Sorowka and Joachim Huth for the SEM analyses and Elmar Gröner for technical support on the NanoSIMS. The Murchison sample (sample ME 2644 spp. #28.21) was provided by the Field Museum Chicago. KL acknowledges support from NSF AST 0807356. Constructive and helpful reviews by Larry Nittler and an anonymous referee helped to improve this manuscript.

Editorial Handling—Dr. Ian Franchi

REFERENCES

Amari S., Anders E., Virag A., and Zinner E. 1990. Interstellar graphite in meteorites. *Nature* 345:238–240.

Amari S., Lewis R. S., and Anders E. 1994. Interstellar grains in meteorites: I. Isolation of SiC, graphite, and diamond; size distributions of SiC and graphite. *Geochimica et Cosmochimica Acta* 58:459–470.

Amari S., Hoppe P., Zinner E., and Lewis R. S. 1995. Trace-element concentrations in single circumstellar silicon carbide grains from the Murchison meteorite. *Meteoritics* 30:679–693.

Amari S., Gao X., Nittler L. R., and Zinner E. 2001a. Presolar grains from novae. *The Astrophysical Journal* 551:1065–1072.

Amari S., Nittler L. R., Zinner E., Gallino R., Lugaro M., and Lewis R. S. 2001b. Presolar SiC grains of type Y: Origin from low-metallicity AGB stars. *The Astrophysical Journal* 546:248–266.

Amari S., Nittler L. R., Zinner E., Lodders K., and Lewis R. S. 2001c. Presolar SiC grains of type A and B: Their isotopic compositions and stellar origins. *The Astrophysical Journal* 559:463–483.

Asplund M., Lambert D. L., Kipper T., Pollacco D., and Shetrone M. D. 1999. The rapid evolution of the born-again giant Sakurai's object. *Astronomy & Astrophysics* 343:507–518.

Bernatowicz T., Fraundorf G., Ming T., Anders E., Wopenka B., Zinner E., and Fraundorf P. 1987. Evidence for interstellar SiC in the Murray carbonaceous meteorite. *Nature* 330:728–730.

Bernatowicz T., Amari S., Zinner E., and Lewis R. S. 1991. Interstellar grains within interstellar grains. *The Astrophysical Journal* 373:L73–L76.

Besmehn A. and Hoppe P. 2003. A NanoSIMS study of Si- and Ca-Ti-isotopic compositions of presolar silicon carbide grains from supernovae. *Geochimica et Cosmochimica Acta* 67:4693–4703.

Chen H.-L. and Schmid-Fetzer R. 2012. The Mg-C phase equilibria and their thermodynamic basis. *International Journal of Materials Research* 103:1294–1301.

Cristallo S., Straniero O., Gallino R., Piersanti L., Dominguez I., and Lederer M. T. 2009. Evolution, nucleosynthesis, and yields of low-mass asymptotic giant branch stars at different metallicities. *The Astrophysical Journal* 696(1): 797–820.

Croat T. K., Bernatowicz T. J., Amari S., Messenger S., and Stadermann F. J. 2003. Structural, chemical, and isotopic microanalytical investigations of graphite from supernovae. *Geochimica et Cosmochimica Acta* 67:4705–4725.

Ding T., Valkiers S., Kipphardt H., De Bievre P., Taylor P. D. P., Gonfiantini R., and Krouse H. R. 2001. Calibrated sulfur isotope abundance ratios of three IAEA sulfur reference materials and V-CDT with a re-assessment of the atomic weight of sulfur. *Geochimica et Cosmochimica Acta* 65:2433–2437.

Fujiya W., Hoppe P., Zinner E., Pignatari M., and Herwig F. 2013. Evidence for radiogenic sulfur-32 in type AB presolar silicon carbide grains? *The Astrophysical Journal Letters* 776:L29 (6 pp).

Gyngard F., Amari S., Zinner E., Gallino R., and Lewis R. S. 2007. Lithium, boron, and sulphur isotopic ratios in large presolar SiC grains from Murchison (abstract #1963). 38th Lunar and Planetary Science Conference. CD-ROM.

Gyngard F., Nittler L. R., and Zinner E. 2010. Presolar SiC of Type C. *Meteoritics & Planetary Science* 45:A72.

Holzapfel C., Soldera F., Vollmer C., Hoppe P., and Mücklich F. 2008. TEM foil preparation of sub-um sized individual grains by focused ion beam technique. *Journal of Microscopy* 235:59–66.

Hoppe P., Annen P., Strebel R., Eberhardt P., Gallino R., Lugaro M., Amari S., and Lewis R. S. 1997. Meteoritic silicon carbide grains with unusual Si-isotopic compositions: Evidence for an origin in low-mass metallicity asymptotic giant branch stars. *The Astrophysical Journal* 487:L101–L104.

Hoppe P., Strebel R., Eberhardt P., Amari S., and Lewis R. S. 2000. Isotopic properties of silicon carbide X grains from the Murchison meteorite in the size range 0.5-1.5 um. *Meteoritics & Planetary Science* 35:1157–1176.

Hoppe P., Lodders K., Strebel R., Amari S., and Lewis R. S. 2001. Boron in presolar silicon carbide grains from supernovae. *The Astrophysical Journal* 551:478–485.

Hoppe P., Fujiya W., and Zinner E. 2012. Sulfur molecule chemistry in supernova ejecta recorded by silicon carbide stardust. *The Astrophysical Journal* 745:L26.

Hoppe P., Cohen S., and Meibom A. 2013. NanoSIMS: Technical aspects and applications in cosmochemistry and biological geochemistry. *Geostandards and Geoanalytical Research* 37:111–154.

Hoppe P., Lodders K., Fujiya W., and Gröner E. 2014. Sulfur in presolar silicon carbide grains from asymptotic giant branch stars (abstract 1031). 45th Lunar and Planetary Science Conference. CD-ROM.

Hutcheon I. D., Huss G. R., Fahey A. J., and Wasserburg G. J. 1994. Extreme ^{26}Mg and ^{17}O enrichments in an Orgueil corundum: Identification of a presolar oxide grain. *The Astrophysical Journal* 425:L97–L100.

Hynes M. K. and Gyngard F. 2009. The presolar grain data base: http://presolar.wustl.edu/~pgd (abstract #1398). 40th Lunar and Planetary Science Conference. CD-ROM.

Hynes K. M., Amari S., Bernatowicz T. J., and Lebsack E. 2010. Microstructural analysis of subgrains in SiC grains of type AB (abstract #5298). In *73rd Annual Meeting of the Meteoritical Society*. Houston, Texas: Lunar and Planetary Institute.

Hynes M. K., Amari S., Bernatowicz T. J., Lebsack E., Gyngard F., and Nittler L. R. 2011. Combined TEM and NanoSIMS analysis of subgrains in a SiC AB grain (abstract #2332). 42th Lunar and Planetary Science Conference. CD-ROM.

Jochum K. P., Weis U., Stoll B., Kuzmin D., Yang Q., Raczek I., Jacob D. E., Stracke A., Birbaum K., Frick D. A., Günther D., and Enzweiler J. 2011. Determination of reference values for NIST SRM 610–617 glasses following ISO guidelines. *Geostandards and Geoanalytical Research* 35(4):397–429.

Kobayashi C., Karakas A. I., and Umeda H. 2011. The evolution of isotope ratios in the Milky Way galaxy. *Monthly Notices of the Royal Astronomical Society* 414:3231–3250.

Lambert D. L., Gustafsson B., Eriksson K., and Hinkle K. H. 1986. The chemical composition of carbon stars. I. Carbon, nitrogen, and oxygen in 30 cool carbon stars in the galactic disk. *The Astrophysical Journal Supplement* 62:373–425.

Lin Y., Gyngard F., and Zinner E. 2010. Isotopic analysis of supernova SiC and Si_3N_4 grains from the Qingzhen (EH3) chondrite. *The Astrophysical Journal* 709:1157–1173.

Lindberg D. and Chartrand P. 2009. Thermodynamic evaluation and optimization of the (Ca+C+O+S) system. *Journal of Chemical Thermodynamics* 41:1111–1124.

Lodders K. and Fegley B. J. 1995. The origin of circumstellar silicon carbide grains found in meteorites. *Meteoritics* 30:661–678.

Lugaro M., Davis A. M., Gallino R., Pellin M. J., Straniero O., and Käppeler F. 2003. Isotopic compositions of strontium, zirconium, molybdenum, and barium in single presolar SiC grains and asymptotic giant branch stars. *The Astrophysical Journal* 593:486–508.

Mauersberger R., Ott U., Henkel C., Cernicharo J., and Gallino R. 2004. The abundance of ^{36}S in IRC+10216 and its production in the galaxy. *Astronomy & Astrophysics* 426: 219–227.

Messenger S., Keller L. P., Stadermann F., Walker R. M., and Zinner E. 2003. Samples of stars beyond the solar system: Silicate grains in interplanetary dust. *Science* 300:105–108.

Nicolussi G. K., Davis A. M., Pellin M. J., Lewis R. S., Clayton R. N., and Amari S. 1997. *s*-Process zirconium in presolar silicon carbide grains. *Science* 277:1281–1283.

Nittler L. R. and Dauphas N. 2006. Meteorites and the chemical evolution of the Milky Way. In *Meteorites and the early solar system II*, edited by Lauretta D. S. and McSween H. Y. Tucson, Arizona: University of Arizona Press. pp. 127–146.

Nittler L. R., Alexander C. M. O'D., Gao X., Walker R. M., and Zinner E. K. 1994. Interstellar oxide grains from the Tieschitz ordinary chondrite. *Nature* 370:443–446.

Nittler L. R., Hoppe P., Alexander C. M. O'D., Amari S., Eberhardt P., Gao X., Lewis R. S., Strebel R., Walker R. M., and Zinner E. 1995. Silicon nitride from supernovae. *The Astrophysical Journal* 453:L25–L28.

Nittler L. R., Amari S., Zinner E., Woosley S. E., and Lewis R. S. 1996. Extinct ^{44}Ti in presolar graphite and SiC: Proof of a supernova origin. *The Astrophysical Journal* 462:L31–L34.

Olofsson H., Eriksson K., and Gustasson B. 1990. A comparison of photospheric and circumstellar [HCN]/[CO]-ratios for bright carbon stars. *Astronomy & Astrophysics* 230:405–411.

Pignatari M., Zinner E., Bertolli M. G., Trappitsch R., Hoppe P., Rauscher T., Fryer C., Herwig F., Hirschi R., Timmes F. X., and Thielemann F.-K. 2013. Silicon carbide grains of type c provide evidence for the production of the unstable isotope 32si in supernovae. *The Astrophysical Journal* 771:L7 (5 pp).

Rauscher T., Heger A., Hoffman R. D., and Woosley S. E. 2002. Nucleosynthesis in massive stars with improved nuclear and stellar physics. *The Astrophysical Journal* 576:323–348.

Slodzian G., Chaintreau M., Dennebouy R., and Rousse A. 2001. Precise in-situ measurements of isotopic abundances with pulse counting of sputtered ions. *European Physical Journal Applied Physics* 14:199–231.

Tang M. and Anders E. 1988. Isotopic anomalies of Ne, Xe, and C in meteorites. II. Interstellar diamond and SiC: Carriers of exotic noble gases. *Geochimica et Cosmochimica Acta* 52:1235–1244.

Timmes F. X., Woosley S. E., and Weaver T. A. 1995. Galactic chemical evolution: Hydrogen through zinc. *The Astrophysical Journal Supplement* 98:617–658.

Tyne V. H., Evans A., Geballe T. R., Eyres S. P. S., Smalley B., and Duerbeck H. W. 2002. Sakurai's Object (V4334 Sgr): Evolution of the dust shell from 1999 to 2001. *Monthly Notices of the Royal Astronomical Society* 334(4):875–882.

Wilson R. G., Stevie F. A., and Magee C. W. 1989. *Secondary ion mass spectrometry: A practical handbook for depth profiling and bulk impurity analysis*. New York: J. Wiley & Sons. 225 p.

Xu Y. C., Amari S., Gyngard F., Zinner E., and Lin Y. 2012. Isotopic measurements of rare submicrometer-sized SiC grains from the Murchison meteorite. *Meteoritics & Planetary Science* 47:5104.

Zega T. J., Nittler L. R., Busemann H., Hoppe P., and Stroud R. M. 2007. Coordinated isotopic and mineralogic analyses of planetary materials enabled by in situ lift-out with a focused-ion-beam scanning electron microscope. *Meteoritics & Planetary Science* 42:1373–1386.

Zinner E. 2014. Presolar grains. In *Meteorites and cosmochemical processes*, edited by Davis A. M. Amsterdam: Elsevier. pp. 181–213.

Zinner E., Nittler L. R., Gallino R., Karakas A. I., Lugaro M., Straniero O., and Lattanzio J. C. 2006. Silicon and carbon isotopic ratios in AGB stars: SiC grain data, models, and the galactic evolution of the Si isotopes. *The Astrophysical Journal* 650:350–373.

Zinner E., Amari S., Guinness R., Jennings C., Mertz A. F., Nguyen A. N., Gallino R., Hoppe P., Lugaro M., Nittler L. R., and Lewis R. S. 2007. NanoSIMS isotopic analysis of small presolar grains: Search for Si_3N_4 grains from AGB stars and Al and Ti isotopic compositions of rare presolar SiC grains. *Geochimica et Cosmochimica Acta* 71:4786–4813.